Density Functional Calculations of NMR Chemical Shifts with the Inclusion of Spin−Orbit Coupling in Tungsten and Lead Compounds

Antonio Rodriguez-Fortea,† Pere Alemany,† and Tom Ziegler*,‡

Departament de Química Física and Centre Especial de Recerca en Química Teòrica (CERQT), Universitat de Barcelona, Diagonal 647, 08028, Barcelona, Catalunya, Spain, and Department of Chemistry, University of Calgary, Calgary, Alberta, T2N 1N4, Canada

Received: April 12, 1999; In Final Form: July 19, 1999

Both the Pauli spin−orbit Hamiltonian and the relativistic zero order regular approximation (ZORA) have been used in conjunction with the gauge including atomic orbital (GIAO) method based on density functional theory (DFT) to calculate ^{207}Pb and ^{183}W NMR chemical shifts. For the tungsten series WO_3S^{2-}, $WO_2S_2^{2-}$, WOS_3^{2-}, WS_4^{2-}, WO_4^{2-}, $W(CO)_6$, WCl_6 and WF_6, one finds the ^{183}W chemical shift to be dominated by paramagnetic contributions, whereas the Fermi-contact contribution induced by spin−orbit coupling is of less importance. On the other hand, in the lead series Me_3PbCl, Me_3PbBr, Me_3PbI, Me_3PbOMe, Me_3PbSMe, $Me_3PbSeMe$, Me_3PbNEt_2, Me_2PbCl_2, and PbX_4 (X = Cl, Br, I), the Fermi-contact term is the trend setting contribution. It is shown that ZORA in general provides chemical shift in better agreement with experiment than the simpler Pauli spin−orbit scheme.

Introduction

It has, in the past decade, become possible to carry out calculations on NMR chemical shifts[1−4] with increasing accuracy. In this regard, the application of density functional theory (DFT) has been especially useful for compounds containing heavy elements. The use of DFT in NMR calculations has been pioneered by Malkin[5] within the "individual gauge for localized orbitals" approach (IGLO)[3a] and subsequently applied by Kaupp[6] and Bühl.[7d,e] Schreckenbach[8a,b] and Ziegler have more recently presented a method in which the NMR shielding tensor is calculated by combining the "gauge including atomic orbitals" (GIAO) approach[9a,b] with density functional theory (DFT) following earlier work by Seifert[9c,d] et al. A number of applications[10] have shown that the GIAO-DFT scheme is capable of reproducing experimental values for ligand chemical shifts of transition metal complexes[10a,b,e] and chemical shifts of heavy main group elements.[10c,d] The DFT-GIAO scheme has further been extended to include the frozen core approximation.[11a] The DFT-GIAO implementation makes full use of the modern features of DFT in terms of accurate exchange-correlation (XC) energy functionals and large basis sets. The DFT-GIAO method has also been implemented by Rauhut[8c] et al. and Cheeseman[8d] et al. as well as Handy[8e] et al. The DFT-GIAO method has further been used in conjunction with hybride DFT methods[12b] by Bühl[7a−c] as well as Godbout and Oldfield.[12a] Traditional ab initio methods have also been applied by Nakatsuji[3c,13] et al. to the calculation of NMR chemical shifts in compounds containing heavy elements.

A special feature of heavier elements is the importance of relativistic effects. Earlier work made use of the Pauli Hamiltonian and demonstrated that both scalar-relativistic terms[10d,11a,14] as well as spin−orbit coupling[15,16] can contribute significantly to the NMR chemical shift. More recently, Wolff[16b] et al. have made use of the variationally more stable relativistic zero order regular approximation (ZORA) by van Lenthe[17] et al. in calculations of NMR chemical shifts.

The objective of the present investigation is to apply both the Pauli and the ZORA Hamiltonian to GIAO-DFT calculations of the chemical shift for the two heavy nuclei ^{183}W and ^{207}Pb. We shall explore the relative merits of the two approximate relativistic Hamiltonians as well as the relative importance of contributions from the scalar relativistic terms and the spin−orbit coupling.

Computational Details and Methods

All calculations were carried out with the help of the Amsterdam Density Functional program package[18] (ADF) and the associated NMR program written by Schreckenbach[8a,11a−b] and Wolff.[16] Use was made of both the Pauli[16a,19] and the ZORA[16b,17] spin−orbit Hamiltonian.

An extended all-electron basis set of Slater type orbitals (STO) was employed in the ZORA calculation with a double-ζ representation in the core region and a triple-ζ representation in the valence area. This basis set is designated as "ZORA basis set IV" in the ADF package and had one polarization function added. For the compound Me_3PbNEt_2, the 1s cores on carbon and nitrogen were frozen for the sake of economy. In the evaluation of the ^{207}Pb chemical shift of this compound, we have used the NMR shielding of the reference, $PbMe_4$, calculated with the same frozen core. The Pauli calculations made use of a basis similar to that employed in the ZORA calculations for O, N, C, and F. For tungsten and lead, the Pauli calculations made use of a triple-ζ STO basis with one polarization function and employed a frozen core up to 4d.

Experimental structures have been used when available. Where experimental geometries were not used, the geometries were optimized employing the scalar-relativistic Pauli method[20] since the direct optimization by ZORA is still under development. The functionals used in the calculation of the molecular orbitals were based on the local density approximation (LDA)

† Universitat de Barcelona.
‡ University of Calgary.

10.1021/jp9912004 CCC: $18.00
Published on Web 09/23/1999

of Vosko, Wilk, and Nusair[21] augmented with Becke's nonlocal exchange correction[22] and Perdew's nonlocal correlation correction.[23] This functional is commonly referred to as BP86.

Experimental ^{183}W NMR shifts with respect to a 2 M solution of Na_2WO_4 are taken from a compilation by Mann.[24] Experimental ^{207}Pb NMR shifts are taken from a compilation by Wrackmeyer and Horchler,[25] where the reference is $PbMe_4$ in a 80% solution of toluene (the ^{207}Pb NMR shift is sensitive to the solvent used in the NMR experiment.)[25]

The NMR shielding tensor for nucleus N can be written as

$$\sigma_{us} = \sigma_{us}^{d} + \sigma_{us}^{p} + \sigma_{us}^{so} = \int \frac{\vec{r}_N \times [\vec{J}_s^{d}(\vec{r}_N) + \vec{J}_s^{p}(\vec{r}_N)]_u}{r_N^3} d\vec{r}_N + \sigma_{us}^{so} \quad (1)$$

Here, $\vec{J}^{d}$ and $\vec{J}^{p}$ are respectively the diamagnetic and paramagnetic current densities[8a] induced by an external magnetic field $\vec{B}_o$ with components $B_{o,s}$. Equation 1 involves an expectation value of r_N^{-3} where r_N is the distance of the reference electron to the NMR nucleus. The paramagnetic current density originates primarily from a coupling between occupied, Ψ_i, and virtual orbitals, Ψ_a, induced by the external magnetic field $\vec{B}_o$,

$$\vec{J}^{p} = \sum_{s=1}^{3} \vec{J}_s^{p} B_{o,s} = \sum_{s=1}^{3} \sum_{i}^{occ} \sum_{a}^{uocc} u_{ai}^{(1,s)} [\Psi_i \vec{\nabla} \Psi_a - \Psi_a \vec{\nabla} \Psi_i] B_{o,s} \quad (2)$$

The principle contribution to the paramagnetic coupling $u_{ai}^{(1)}$ is given by

$$u_{ai}^{(1)} \approx \propto -\frac{1}{2(\epsilon_i^{(0)} - \epsilon_a^{(0)})} \sum_{\lambda,\nu} c_{\lambda a}^{(0)} c_{\nu i}^{(0)} \{\langle \chi_\lambda | [\vec{r}_\nu \times \vec{\nabla}]_u | \chi_\nu \rangle\} \propto -\frac{1}{2(\epsilon_i^{(0)} - \epsilon_a^{(0)})} \langle \Psi_a | \hat{M}_u | \Psi_i \rangle \quad (3)$$

Here $\epsilon^{(0)}$ refers to orbital energies of the unperturbed molecules without the external magnetic field and generated from a ZORA or Pauli calculation with the spin−orbit coupling term included. The term $\langle \Psi_a | \hat{M}_s | \Psi_i \rangle$ represents the first-order magnetic coupling between an occupied molecular orbital, i, and a virtual orbital, a. Within the GIAO formalism,[8a] the action of the magnetic operator $\hat{M}_s$ on Ψ_q is simply to work with $i\hat{L}_s^{\nu}$ on each atomic orbital χ_ν. Here $\hat{L}_u^{\nu}$ is the s-component of the angular momentum operator with its origin at the center $\vec{R}_\nu$ on which χ_ν is situated. Tabulations for $\hat{L}_u^{\nu}\chi_\nu$ are available in the literature.[27,28]

The spin−orbit contribution to the chemical shift, $\sigma_{\lambda\nu}^{so}$, is dominated by the Fermi-contact term[16a]

$$\sigma_{us}^{so} \cong \sigma_{us}^{FC} = \frac{4\pi g}{3c} \sum_{i}^{occ} \sum_{a}^{vir} u_{ia}^{(1,s)} \langle \Psi_a | \hat{S}_u \delta(r_N = 0) | \Psi_i \rangle \quad (4)$$

where $\hat{S}_u$ is a Cartesian component of the electronic spin operator, c is the speed of light, and g is the electronic Zeeman g-factor. A full account of all terms in $\sigma_{\lambda\nu}^{so}$ can be found elsewhere.[16a,b]

Results and Discussion

^{183}W NMR Shifts. We shall now present results from calculations of ^{183}W NMR chemical shifts in which we have applied either the ZORA-NMR formulation[16b] or the corresponding Pauli-NMR scheme[16a] (PSO), in both cases with full inclusion of the spin−orbit coupling term.

TABLE 1: Geometries Used in the Calculations of Tungsten Compounds (Lengths in Å, Angles in Degrees)[e]

system	geometry	method	structural parameters
WO_4^{2-}	experimental[a]	X-ray diffr.	r(W−O) = 1.79, tetrahedral
WO_3S^{2-}	optimized	SR/BP86	r(W−O) = 1.7897 (avg), r(W−S) = 2.3262 ∠(S−W−O) = 110.5 (avg)
$WO_2S_2^{2-}$	optimized	SR/BP86	r(W−O) = 1.7733 (avg), r(W−S) = 2.2786 (avg) ∠(S−W−S) = 113.2, ∠(O−W−O) = 106.8
WOS_3^{2-}	optimized	SR/BP86	r(W−O) = 1.7598, r(W−S) = 2.2549 (avg) ∠(O−W−S) = 108.4 (avg)
WS_4^{2-}	optimized	SR/BP86	r(W−S) = 2.2312, tetrahedral
WCl_6	experimental[b]	gas electron diffr	r(W−Cl) = 2.2893, octahedral
WF_6	experimental[c]	gas electron diffr	r(W−F) = 1.833, octahedral
$W(CO)_6$	experimental[d]	X-ray diffr	r(W−C) = 2.058, r(C−O) = 1.148, octahedral

[a] Reference 26a. [b] Reference 26b. [c] Reference 26c. [d] Reference 26d. [e] "SR/BP86" corresponds to scalar-relativistic optimization using the BP86 functional; "avg" = averaged.

To our knowledge, the only other detailed calculations of tungsten NMR shifts including spin−orbit coupling have been carried out by Nakatsuji[15c] et al. They calculated the shifts of tungsten-hexafluoride, -hexachloride, and -tetraoxide using the tungsten hexafluoride as the reference. We have in addition considered the NMR chemical shift of the W(VI) compounds WO_3S^{2-}, $WO_2S_2^{2-}$, WOS_3^{2-}, and WS_4^{2-} as well as the W(0) compound $W(CO)_6$. We have used WO_4^{2-} as the reference in order to be able to compare with the experimental NMR shifts compiled by Mann.[24]

There is a great number of tungsten compounds whose ^{183}W NMR shifts have been recorded experimentally and they exhibit a wide variation in the chemical shift from 4700 to −4700 ppm. Thus, the range of tungsten NMR is approximately 9400 ppm. The experimental range for the chemical shifts we are studying is about 7200 ppm.

In the tables that follow, δ^{p} and δ^{d} are the paramagnetic and the diamagnetic contributions, respectively, to the total calculated chemical shift, δ^{cal}. Further, δ^{FC} is the Fermi-contact contribution[16a] in the Pauli formalism induced by the spin−orbit coupling and δ^{SO} is the corresponding contribution from the spin−orbit coupling in the ZORA formulation[16b] with the major part coming again from the Fermi-contact term of eq 4. Furthermore, δ^{exp} is the experimental chemical shift.

The calculated shift is evaluated as

$$\delta^{cal}(\text{sample}) = \sigma^{cal}(WO_4^{2-}) - \sigma^{cal}(\text{sample})$$

where $\sigma^{cal}(WO_4^{2-})$ and σ^{cal}(sample) are the NMR isotropic shieldings of the reference (WO_4^{2-}) and of the sample in question, respectively. Finally, "diff" is the absolute difference between δ^{cal} and δ^{exp}. All chemical shifts are in ppm, all bond lengths in angstroms (Å), and all the angles are in degrees (°).

Table 1 presents the structural parameters used in the calculations. Some of the structures are experimental,[26] WO_4^{2-}, WF_6, WCl_6, and $W(CO)_6$, and the other are optimized, WO_3S^{2-}, $WO_2S_2^{2-}$, WOS_3^{2-}, and WS_4^{2-}.

TABLE 2: Different Contributions to the ^{183}W NMR Chemical Shift in the ZORA and PSO Formalisms

	δ^{para}		δ^{dia}		δ^{SO}/δ^{FC}		δ^{cal}			diff	
system	ZORA	PSO	ZORA	PSO	ZORA	PSO	ZORA	PSO	δ^{exp}	ZORA	PSO
WO_3S^{2-}	798.48	736.95	−1.07	−1.55	23.08	−11.88	820.49	723.52	841[a]	21	117
$WO_2S_2^{2-}$	1613.73	1468.50	−1.94	5.85	51.71	−21.47	1663.49	1452.88	1787[a]	124	334
WOS_3^{2-}	2543.57	2292.78	−2.92	−4.26	76.28	−30.00	2616.93	2258.52	2760[a]	143	501
WS_4^{2-}	3541.25	3160.60	−3.88	−6.17	101.04	−32.98	3638.41	3121.45	3769[a]	131	648
WCl_6	2019.37	1853.79	−7.88	−8.64	−79.02	−72.61	1932.47	1772.54	2181[b]	249	408
WF_6	−570.60	−126.10	9.91	27.94	−69.49	−8.81	−630.19	−106.97	−1121[b]	491	1014
$W(CO)_6$	−3667.81	−3825.30	−11.41	−12.65	−196.92	−7.68	−3876.14	−3305.63	−3446[c]	430	140
abs mean										227	452

[a] References 24a,c. [b] References 24a,b. [c] References 24a,d.

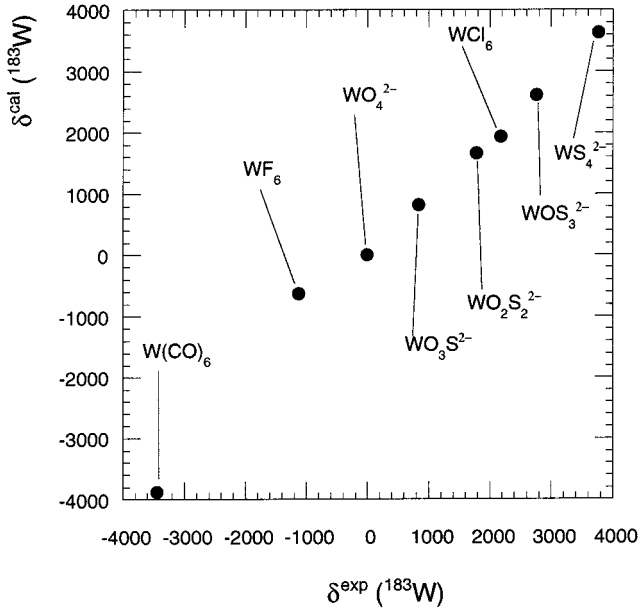

Figure 1. Calculated (ZORA formalism) versus experimental ^{183}W chemical shifts.

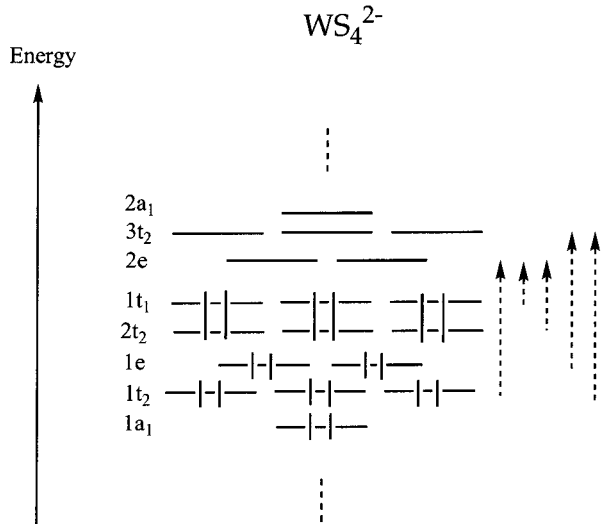

Figure 2. Qualitative representation of part of the molecular orbital energetic diagram for WS_4^{2-} compound, showing also the most important transitions between occupied and virtual molecular orbitals that contribute to the paramagnetic shielding.

The ^{183}W NMR shifts evaluated by the ZORA-NMR and Pauli-NMR methods with spin−orbit coupling included are presented in Table 2. Both ZORA-NMR and Pauli-NMR are able to reproduce the trends in the experimental NMR chemical shifts qualitatively. However, results from the ZORA method agree better with experiment than the data obtained by the Pauli scheme. The average absolute difference of the ZORA NMR chemical shifts with respect to experiment is 227 ppm compared to 452 ppm for the Pauli NMR chemical shifts. Thus, ZORA with the more elaborate relativistic treatment is seen to afford the more accurate estimate of chemical shifts for the heavy ^{183}W nuclei.

The good agreement between experiment and theory for ZORA-NMR is depicted in Figure 1 where δ^{cal} (ZORA results) is plotted against δ^{exp}. The average absolute deviation of 227 ppm represents 3% of the experimental range (7200 ppm) for the ^{183}W chemical shift of the calculated compounds.

It follows from Table 2 that the small and almost constant diamagnetic contribution, δ^{d}, to the chemical shift has a negligible influence on the observed trends for δ^{cal} and δ^{exp}. This is understandable since the diamagnetic shielding largely comes from constant core terms that are the same in the different tungsten compounds and thus cancel out in the expression of the chemical shift. The chemical shift is instead dominated by the paramagnetic contribution. The magnitude of the paramagnetic shielding is largely determined by the u_{ia} matrix of eq 3. Components of this matrix are proportional to the coupling of occupied (i) and virtual (a) orbitals by the magnetic field and inversely proportional to the energy difference between these orbitals, eq 3.

The spin−orbit contribution to the chemical shift, σ_{us}^{so} of eq 4, is not very important for the tungsten compounds considered here; see Table 2. As discussed elsewhere,[15b,16a] σ_{us}^{so} for central atoms are important if they are coordinated to elements with large spin−orbit constants (Se, Te, Br, I, etc.) through bonds that contain a significant contribution from the s orbitals on the central atom. This is not the case here where sulfur is the heaviest ligand element and the bonding role of the 6s tungsten orbital is modest.

It is clear from Table 2 that the chemical shift for the tetrahedral complexes decreases from WS_4^{2-} as more and more sulfurs are replaced by oxygens. It also follows from Table 2 that this trend is set by δ^{p}. We can understand the dependence of δ^{p} on the number of oxygens by considering the frontier orbital diagram for WS_4^{2-}; see Figure 2. The occupied frontier orbitals consist of a set of metal−ligand bonding orbitals (2a, $1t_2$, 1e) with a predominant ligand component as well as a set of ligand-based lone pair orbitals ($1t_1$, $2t_2$). The lowest unoccupied orbitals are the corresponding ligand−metal antibonding orbitals ($2a_1$, $3t_2$, 2e) with a predominant metal component. The paramagnetic contribution δ^{p} originates primarily from magnetic couplings between the metal−ligand bonding orbitals ($1t_2$, 1e) and the corresponding ligand−metal antibonding orbitals ($3t_2$, 2e); see Figure 2. As sulfur is replaced by the more electronegative oxygens the predominantly ligand-based metal−ligand

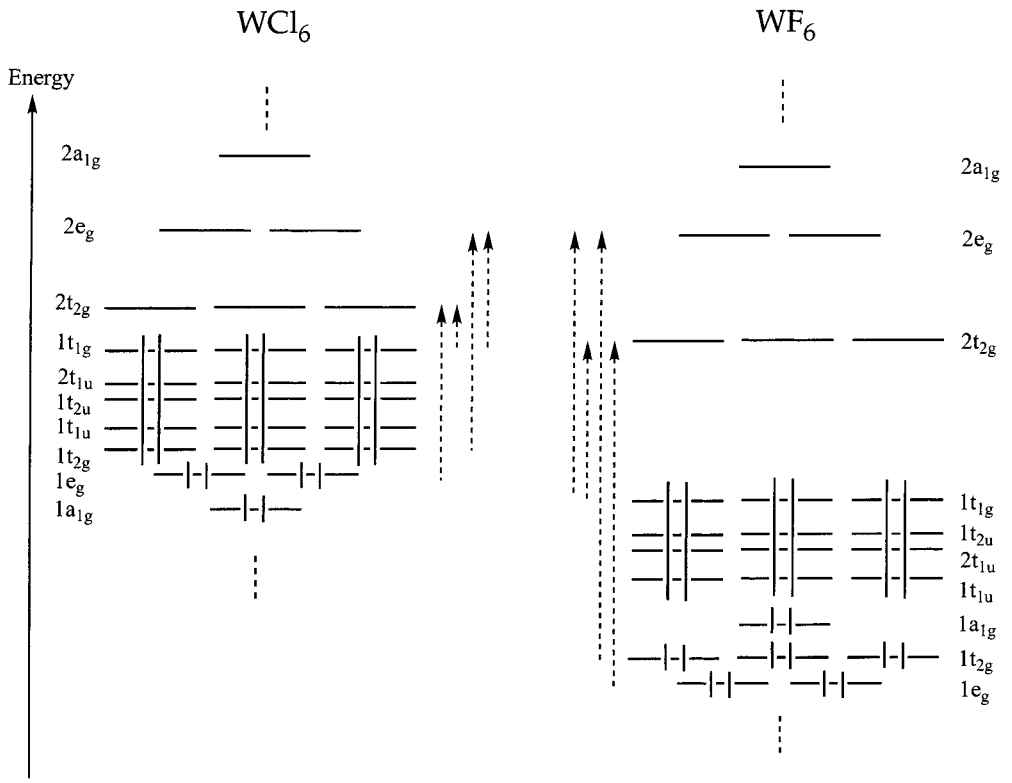

Figure 3. Qualitative comparison of molecular orbital energetic diagram for the W(VI) octahedral compounds, WF_6 and WCl_6, showing also the most important transitions between occupied and virtual molecular orbitals that contribute to the paramagnetic shielding.

bonding orbitals are lowered relative to the predominantly metal based metal−ligand antibonding orbitals, leading to a larger energy gap between bonding and antibonding orbitals. This will in turn results in a smaller paramagnetic contribution δ^p as the coupling matrices $u_{ai}^{(1,s)}$, eq 3, are diminished by the larger energy gap.

For the two tungsten hexahalides, we note as well a decrease in the chemical shift and δ^p toward the species, WF_6 with the more electronegative ligand. As shown in Figure 3, the trend is again determined by an increase in the energy gap between the predominantly ligand-based metal−ligand ($1t_{2g}$ and $1e_g$) orbitals and the predominantly metal-based ligand−metal antibonding orbitals ($2t_{2g}$ and $2e_g$) as the ligand becomes more electronegative.

^{207}Pb NMR Shifts. We have also applied the ZORA-NMR[16b] and the Pauli spin−orbit (PSO) NMR[16a] to the calculation of ^{207}Pb NMR shifts.

To our knowledge these are the first published calculations of lead NMR chemical shifts in which spin−orbit coupling has been taken into account. We have calculated the ^{207}Pb shift of several Pb(IV) compounds: Me_3PbCl, Me_3PbBr, Me_3PbI, Me_3PbOMe, Me_3PbSMe, $Me_3PbSeMe$, Me_3PbNEt_2, Me_2PbCl_2, and $PbCl_4$, using $PbMe_4$ as the reference in order to compare with experimental results.[25] We have also calculated the ^{207}Pb shift for $MePbCl_3$, $PbBr_4$, and PbI_4 in order to explore fully substituent effect on the ^{207}Pb NMR shift, although experimental data are unavailable for these compounds.

The experimental ^{207}Pb chemical shifts values span a range of 9000 ppm for Pb(IV), and the range covered by the compounds we have studied is about 1400 ppm. It is important to note that the observed ^{207}Pb shifts for some of the compounds have been measured in different solvents with somewhat different results. In these cases, our comparison to experiment corresponds to the values measured in the weakly coordinating solvent CH_2Cl_2.

The calculated shift is evaluated as

$$\delta^{cal}(\text{sample}) = \sigma^{cal}(PbMe_4) - \sigma^{cal}(\text{sample})$$

where $\sigma^{cal}(PbMe_4)$ and σ^{cal}(sample) are the isotropic NMR shieldings of the reference ($PbMe_4$) and of the sample in question, respectively. Table 3 presents the structural parameters used in the calculations. All geometries were optimized with the exception of $PbMe_4$ and $PbCl_4$ for which good experimental estimates are available.[29]

The calculated ZORA-NMR and PSO-NMR ^{207}Pb chemical shifts along with their paramagnetic, diamagnetic, and spin−orbit (Fermi-contact) contributions are presented in Table 4. We provide as well the observed values along with the absolute difference (diff) between theory and experiment. As in the case of the tungsten compounds, both ZORA-NMR and PSO-NMR are able to account qualitatively for the experimental trends with ZORA-NMR providing the best fit to experiment. Thus, the ZORA-NMR method is in all cases able to reproduce the sign of the experimental chemical shifts, whereas some PSO shifts have the wrong sign. The average difference between theory and experiment is 60 ppm for ZORA-NMR compared to 251 ppm in the case of PSO-NMR. Thus, in line with the tungsten results, the experimental chemical shifts for ^{207}Pb NMR are best reproduced by the ZORA-NMR formalism.

Figure 4 affords a plot of δ^{cal} versus δ^{exp} based on the ZORA-NMR method. The average absolute deviation of 60 ppm corresponds to 4% of the experimental ^{207}Pb chemical shift range of about 1400 ppm. We have not included Me_2PbCl_2 in the calculated mean absolute deviation (diff = 872 ppm). It is likely[25a] that Me_2PbCl_2 is coordinated with one or more DMSO (dimethyl sulfoxide) solvent molecules.It follows from Table 4 that δ^d is numerically small and nearly constant throughout the series of Pb(IV) compounds as the diamagnetic shielding largely comes from constant core terms that are canceled out in the

TABLE 3: Geometries Used in the Calculations for Lead Compounds (Lengths in Å, Angles in Degrees)

compound	geometry	method	structural parameters
$PbMe_4$	experimental[a]	gas electron diffr.	r(Pb−C) = 2.238, tetrahedral
$PbCl_4$	experimental[a]	gas electron diffr.	r(Pb−Cl) = 2.3693, tetrahedral
Me_3PbCl	optimized	SR/BP86	r(Pb−Cl) = 2.5357, r(Pb−C) = 2.2596 (avg), ∠(Cl−Pb−C) = 99.5 (avg)
Me_3PbBr	optimized	SR/BP86	r(Pb−Br) = 2.6319, r(Pb−C) = 2.2669 (avg), ∠(Br−Pb−C) = 100.7 (avg)
Me_3PbI	optimized	SR/BP86	r(Pb−I) = 2.8721, r(Pb−C) = 2.2705 (avg), ∠(I−Pb−C) = 101.1 (avg)
Me_3PbOMe	optimized	SR/BP86	r(Pb−O) = 2.1577, r(Pb−C) = 2.2721 (avg), r(O−C) = 1.4190, ∠(O−Pb−C) = 101.4 (avg)
Me_3PbSMe	optimized	SR/BP86	r(Pb−S) = 2.5898, r(Pb−C) = 2.2746 (avg), r(S−C) = 1.8403, ∠(S−Pb−C) = 102.5 (avg)
$Me_3PbSeMe$	optimized	SR/BP86	r(Pb−Se) = 2.6595, r(Pb−C) = 2.2794 (avg), r(Se−C) = 1.9837, ∠(Se−Pb−C) = 106.2 (avg)
Me_3PbNEt_2	optimized	SR/BP86	r(Pb−N) = 2.2163, r(Pb−C) = 2.2831 (avg), r(N−C) = 1.4677 (avg)
Me_2PbCl_2	optimized	SR/BP86	r(Pb−Cl) = 2.4903 (avg), r(Pb−C) = 2.2399 (avg), ∠(Cl−Pb−Cl) = 104.5, ∠(C−Pb−C) = 129.7
$MePbCl_3$	optimized	SR/BP86	r(Pb−Cl) = 2.4676 (avg), r(Pb−C) = 2.2455, ∠(C−Pb−Cl) = 112.8
$PbBr_4$	optimized	SR/BP86	r(Pb−Br) = 2.5739 (avg), tetrahedral
PbI_4	optimized	SR/BP86	r(Pb−I) = 2.8219 (avg), tetrahedral

[a] Reference 29. [b] "SR/BP86" corresponds to scalar-relativistic optimization using the BP86 functional. "avg" = averaged.

TABLE 4: Different Contributions to the ^{207}Pb NMR Chemical Shift in the ZORA and PSO Formalisms

	δ^{para}		δ^{dia}		δ^{SO}/δ^{FC}		δ^{cal}			diff	
compound	ZORA	PSO	ZORA	PSO	ZORA	PSO	ZORA	PSO	δ^{exp}	ZORA	PSO
Me_3PbCl	435.58	271.33	0.64	0.91	91.64	−62.28	527.86	209.96	432.0[a]	95.9	222.0
Me_3PbBr	414.70	231.23	1.04	1.15	−104.61	−220.75	311.13	11.63	367.0[a]	55.9	355.4
Me_3PbI	501.03	344.72	−0.95	−0.30	−414.34	−524.08	85.74	−179.66	203.6[a]	117.9	383.3
Me_3PbOMe	287.66	106.66	1.88	2.53	103.84	−32.76	393.38	76.43	331.3[b]	62.1	254.9
Me_3PbSMe	267.17	126.60	−0.13	0.86	28.66	−66.05	295.70	61.41	239.0[a]	56.7	177.6
$Me_3PbSeMe$	289.63	163.44	0.48	1.14	−228.65	−308.85	61.46	−144.27	80.5[c]	19.1	242.3
Me_3PbNEt_2	187.79	5.16	1.34	2.65	81.46	−24.81	270.59	−17.00	242[a]	29	259
Me_2PbCl_2	579.69	391.93	−0.41	0.15	70.54	−183.10	649.82	208.98	−222[d]	872[f]	431[f]
$PbCl_4$	152.20	38.06	−4.52	−4.21	−869.31	−917.49	−721.63	−883.64	−767.7[e]	46.1	115.9
$PbBr_4$	512.99	270.28	−1.26	−0.20	−5336.60	−6298.40	−4824.87	−6028.32			
PbI_4	1155.64	754.56	−8.74	−3.81	−8388.21	−14032.94	−7241.31	−13281.99			
$MePbCl_3$	451.11	257.04	−1.72	−1.02	−256.48	−513.74	192.91	−257.72			
abs. mean										60	251

[a] References 25a,b. [b] References 25a,c. [c] References 25a,d. [d] References 25a,e. [e] References 25a,f. [f] These values are not included in the calculation of the absolute mean difference.

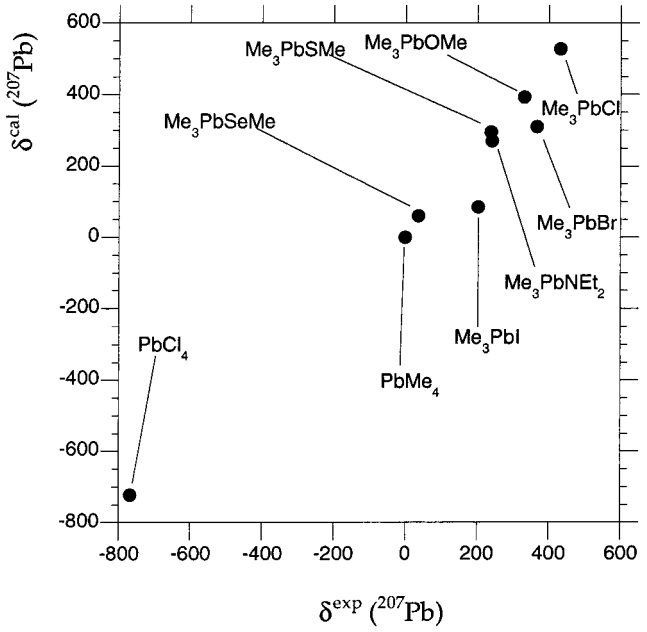

Figure 4. Calculated (ZORA formalism) versus experimental ^{207}Pb chemical shifts.

expression of the chemical shift. Both the paramagnetic (δ^{p}) and the spin−orbit contribution (δ^{so}) are seen to be of importance for the ^{207}Pb shift. The spin−orbit contribution is very sensitive to the atomic number of the atoms directly coordinated to the metal. The heavier the atoms, the larger the absolute value of δ^{so} (δ^{FC}). This is underlined by the Me_3PbX series with X = Cl, Br, and I or X = OMe, SMe, and SeMe, Table 4, and further underlined in the tetrahalide series PbX_4 with X = Cl, Br, and I. We shall in the following provide a more detailed analysis of the calculated trends in the ^{207}Pb shift.

PbX_4 (X = Cl, Br, and I). It follows from Table 4 that the paramagnetic contribution to the chemical shift increases from X = Cl to X = I. An energy level diagram for the valence orbitals of PbX_4 that might be involved in the paramagnetic coupling is shown in Figure 5. The occupied valence orbitals consist of the Pb−X bonding orbitals $1a_1$, $1t_2$, and 1e as well as the halogen lone pair orbitals $2t_2$ and $1t_1$, whereas the lowest unoccupied levels are represented by the Pb−X antibonding orbitals $2a_1$ and $3t_2$. Our analysis indicates that the predominant paramagnetic coupling is between the occupied halogen lone pair orbital $1t_1$ and the Pb−X antibonding orbitals $2a_1$, all other couplings are 5−10 times smaller in magnitude. As we increase the electronegativity of X in going from X = I to X = Cl, both $1t_1$ and $2a_1$ are lowered in energy. However, the nearly pure halogen lone pair orbital $1t_1$ is lowered the most, leading to an increase in the $1t_1$ to $2a_1$ energy gap and a reduction in the paramagnetic coupling. Thus, both the WX_4^{2-} series and the PbX_4 series tend, for much the same reason, toward larger paramagnetic contributions to the chemical shifts as the electronegativity of X is decreased.

The positive δ^{p} term in the PbX_4 series is overshadowed by a numerically much larger negative Fermi-contact contribution δ^{FC}, Table 4, which increases in absolute terms from the lighter chlorine to the heavier iodine. The origin of this term, eq 4, can be understood by observing that the halogens with nearly degenerate lone-pair orbitals $2t_2$ and $1t_1$ increasingly will experience the influence of spin−orbit coupling as we descend the halogen family toward heavier homologous. Placed in a

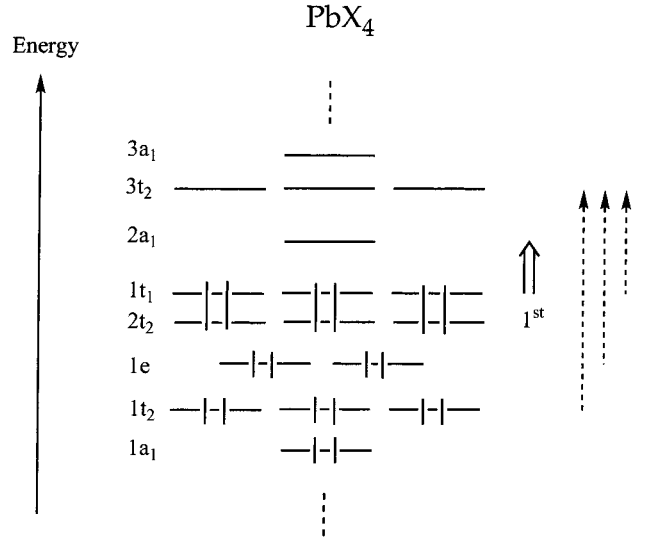

Figure 5. Qualitative representation of the molecular orbital energetic diagram for the PbX_4, X = Cl, Br, and I, tetrahedral compouds, showing also the most important transitions that contribute to the paramagnetic shielding. In this series, the first transition is between 6 and 10 times more important (in each direction of space) than the second one, and it is shown with a different arrow.

magnetic field, the spin−orbit coupling effect will induce[15a−b,d,16a] a net spin density on the halogens with a spin component opposite to the external magnetic field in order to lower the energy. The spin density on the halogens will induce a spin density on the central atom of opposite polarization which in turn will produce an internal magnetic field opposite to the external field in the vicinity of the lead nucleus. The result is an increase in the shielding of lead and a corresponding negative contribution to the chemical shift.

Me_3PbX (X = Cl, Br, and I) and Me_3PbXMe (X = O, S, and Se). These two series nicely underline the principles described above. The paramagnetic coupling is again between occupied π−lone pair orbitals on the ligands and empty Pb−L antibonding orbitals. Further, the paramagnetic coupling δ^p is largest for the less electronegative X as the energy gaps between occupied and virtual orbitals are smallest. Also, δ^{so} (δ^{FC}) is seen to become increasingly negative with heavier representatives for X as spin−orbit coupling become more important. We note that δ^p is dominant for lighter X elements, resulting in positive ^{207}Pb shift, whereas δ^{so} (δ^{FC}) prevails for the heavier X members giving rise to negative ^{207}Pb shifts. It is clear from our analysis that the diamagnetic contribution is of little importance. However, the change toward more negative ^{207}Pb chemical shifts with the less electronegative substituents X has in the past been rationalized in terms of an increase in the electron charge and diamagnetic shielding on lead. We finally note that the ^{207}Pb shift becomes more and more negative for the series $Me_{4-y}PbCl_y$ (y = 0, 1, 2, 3, and 4) as we add chlorines and increase the negative contribution from δ^{so} (δ^{FC}). The substantial error in the calculated shift δ^{cal} for Me_3PbI reflects that δ^{cal} is made up of large contributions of opposite signs from respectively δ^{so} (δ^{FC}) and δ^p.

Concluding Remarks

We have applied the GIAO-DFT method together with both the Pauli spin−orbit Hamiltonian and the relativistic zero order regular approximation (ZORA) in calculations on ^{207}Pb and ^{183}W NMR chemical shifts. We find that ZORA in general provides chemical shift in better agreement with experiment than the simpler Pauli spin−orbit scheme.

The chemical shift in the tungsten series WO_3S^{2-}, $WO_2S_2^{2-}$, WOS_3^{2-}, WS_4^{2-}, WO_4^{2-}, $W(CO)_6$, WCl_6, and WF_6 is determined by the paramagnetic contribution δ^p, whereas the spin−orbit term (δ^{so}) was found to be small. It is shown that δ^p increases from WO_4^{2-} toward WS_4^{2-} since the less electronegative sulfur ligands makes the energy gap between occupied and virtual orbitals involved in the paramagnetic coupling smaller. A similar trend with respect to the electronegativity of the ligand is observed for the series WF_6 and WCl_6.

In the lead series: Me_3PbCl, Me_3PbBr, Me_3PbI, Me_3PbOMe, Me_3PbSMe, $Me_3PbSeMe$, Me_3PbNEt_2, Me_2PbCl_2, and PbX_4 (X = Cl, Br, I), we find the spin−orbit (δ^{so}) induced Fermi-contact term to be trend setting. It is argued that this term should be increasingly negative as the ligand X atom in the series Me_3PbX (X = Cl, Br, I), Me_3PbXMe (X = O, S, Se), and PbX_4 (X= Cl, Br, I) becomes heavier. The change toward more negative ^{207}Pb chemical shifts with the heavier, less electronegative substituents X has in the past been rationalized in terms of an increase in the electron charge and diamagnetic shielding on lead. This interpretation is incorrect since our calculations demonstrate that δ^d is small and constant for all the investigated lead compounds.

Acknowledgment. This work was supported by the National Sciences and Engineering Research Council of Canada (NSERC) and DGES (Spain) through Project PB95-0848-C02-01. T.Z. acknowledges a Canada Council Killam Research Fellowship. A.R.F. thanks CIRIT (Generalitat de Catalunya) for a doctoral grant and for financial support for his stay in the University of Calgary. We thank Dr. S. Wolff for help and useful discussions.

References and Notes

(1) (a) *Multinuclear NMR*; Mason, J., Ed.; Plenum Press: New York, 1987. (b) Fukui, H. *Magn. Reson. Rev.* **1987**, *11*, 205. (c) Chesnut, D. B. In *Annual Reports on NMR Spectroscopy*; Webb, G. A., Ed.; Academic Press: New York, 1989; Vol. 21. (d) Jameson, C. J. In *Specialist Periodic Reports on NMR*; Webb, G. A., Ed.; Royal Society of Chemistry: London, 1980−1997; Vols. 8−26. (e) Pyykkö, P. *Chem. Rev.* **1988**, *88*, 563.

(2) (a) *Nuclear Magnetic Shieldings and Molecular Structure*; Tossell, J. A., Ed.; NATO ASI C386; Kluwer Academic Publishers: Dordrecht, The Netherlands, 1993. (b) Chesnut, D. B. In *Annual Reports on NMR Spectroscopy*; Webb, G. A., Ed.; Academic Press: New York, 1994; Vol. 29.

(3) (a) Kutzelnigg, W.; Fleischer, U.; Schindler, M. In *NMR−Basic Principles and Progress*; Springer-Verlag: Berlin, 1990; Vol. 23, p 165. (b) Wolinski, K.; Hilton, J. F.; Pulay, P. *J. Am. Chem. Soc.* **1990**, *112*, 8251. (c) Ballard, C. C.; Hada, M.; Nakatsuji, H. *Chem. Phys. Lett.* **1995**, *254*, 170.

(4) Gauss, J.; Stanton, J. F. *J. Chem. Phys.* **1995**, *102*, 251.

(5) (a) Malkin, V. G.; Malkina, O. L.; Erikson, L. A.; Salahub, D. R. In *Modern Density Functional Theory: A Tool for Chemistry*; Politzer, P., Seminario, J. M., Eds.; Elsevier: Amsterdam, The Netherlands, 1995; Vol. 2. (b) Malkin, V. G.; Malkina, O. L.; Salahub, D. R. *Chem. Phys. Lett.* **1995**, *239*, 186. (c) Malkin, V. G.; Malkina, O. L.; Salahub, D. R. *Chem. Phys. Lett*. **1996**, *261*, 335.

(6) (a) Kaupp, M.; Malkin, V. G.; Malkina, O. L.; Salahub, D. R. *J. Am. Chem. Soc.* **1995**, *117*, 1851. (b) Kaupp, M.; Malkin, V. G.; Malkina, O. L.; Salahub, D. R. *Chem. Phys. Lett.* **1995**, *235*, 382. (c) Kaupp, M.; Malkin, V. G.; Malkina, O. L.; Salahub, D. R. *Chem.−Eur. J.* **1996**, *2*, 24. (d) Kaupp, M. *Chem.−Eur. J.* **1996**, *2*, 348. (e) Kaupp, M. *Chem. Ber.* **1996**, *129*, 527. (f) Kaupp, M. *Chem. Ber.* **1996**, *129*, 535. (g) Kaupp, M. *J. Am. Chem. Soc.* **1996**, *118*, 3018. (h) Kaupp, M.; Malkina, O. L.; Malkin, V. G. *Chem. Phys. Lett.* **1997**, *265*, 55.

(7) (a) Bühl, M. *Organometallics* **1997**, *16*, 251. (b) Bühl, M. *Chem. Phys. Lett.* **1997**, *267*, 251. (c) Bühl, M. *J. Phys. Chem. A.* **1997**, *101*, 2514. (d) Bühl, M.; Brintzinger, H−H.; Hopp, G. *Organometallics* **1996**, *15*, 778. (e) Bühl, M.; Malkin, V. G.; Malkina, O. L.; *Helv. Chim. Acta* **1996**, *79*, 742. (f) Bühl, M. *J. Phys. Chem. A* **1997**, *101*, 2514.

(8) (a) Schreckenbach, G.; Ziegler, T. *J. Phys. Chem.* **1995**, *99*, 606. (b) Schreckenbach, G.; Dickson, R. M.; Ruiz-Morales, Y.; Ziegler, T. In *Density Functional Theory in Chemistry*; Laird, B., Ross, R., Ziegler, T., Eds.; American Chemical Society: Washington, DC, 1996; p 328. (c) Rauhut, G.; Puyear, S.; Wolinski, K.; Pulay, P. *J. Phys. Chem.* **1996**, *100*,

6130. (d) Cheeseman, J. R.; Trucks, G. W.; Keith, T. A.; Frisch, M. J. *J. Chem. Phys.* **1996**, *104*, 5497. (e) Lee, A. M.; Handy, N. C.; Colwell, S. M. *J. Chem. Phys.* **1995**, *103*, 10095. (f) Schreckenbach, G.; Ziegler, T. *Theor. Chem. Acc.* **1998**, *99*, 71.

(9) (a) London, F. *J. Phys. Radium* **1937**, *8*, 397. (b) Ditchfield, R. *Mol. Phys.* **1974**, *27*, 789. (c) Bieger, W.; Seifert, G.; Eschrig, H.; Grossmann, G. *Chem. Phys. Lett.* **1985**, *115*, 275. (d) Friedrich, K.; Seifert, G.; Grossmann, G. *Z. Phys.* **1990**, *D17*, 45.

(10) (a) Ruiz-Morales, Y.; Schreckenbach, G.; Ziegler, T. *J. Phys. Chem.* **1996**, *100*, 3359. (b) Ruiz-Morales, Y.; Schreckenbach, G.; Ziegler, T. *Organometallics* **1996**, *15*, 3920. (c) Ruiz-Morales, Y.; Schreckenbach, G.; Ziegler, T. *J. Phys. Chem.* **1997**, *101*, 4121. (d) Schreckenbach, G.; Ruiz-Morales, Y.; Ziegler, T. *J. Chem. Phys.* **1996**, *104*, 8605. (e) Ehlers, A. W.; Ruiz-Morales Y.; Baerends, E. J.; Ziegler, T. *Inorg. Chem* **1997**, *36*, 5031.

(11) (a) Schreckenbach, G.; Ziegler, T. *Int. J. Quantum Chem.* **1996**, *60*, 753. (b) Schreckenbach, G.; Ziegler, T. *Int. J. Quantum Chem.* **1997**, *61*, 899.

(12) (a) Godbout, N.; Oldfield, E. *J. Am. Chem. Soc.* **1997**, *119*, 8065. (b) Becke, A. D. *J. Chem. Phys.* **1993**, *98*, 5648.

(13) (a) Nakatsuji, H.; Takashima, H.; Hada, M. *Chem. Phys. Lett.* **1995**, *233*, 95. (b) Nakatsuji, H.; Nakajima, T.; Hada, M.; Takashima, H.; Tanaka, S. *Chem. Phys. Lett.* **1995**, *247*, 418. (c) Nakatsuji, H.; Hada, M.; Tejima, T.; Nakajima, T.; Sugimoto, M. *Chem. Phys. Lett.* **1995**, *249*, 284.

(14) Kaupp, M.; Malkin, V. G. *J. Chem. Phys.* **1997**, *106*, 9201.

(15) (a) Cheremisin, A. A.; Schastnev, P. V. *J. Magn. Reson.* **1980**, *40*, 459. (b) Kaupp, M.; Malkina, O. L.; Malkin, V. G.; Pyykkö, P. *Chem.—Eur. J.* **1998**, *4*, 118. (c) Hada, M.; Kaneko, H.; Nakatsuji, H. *Chem. Phys. Lett.* **1996**, *261*, 7. (d) Morishima, I.; Endo, K.; Yonezawa, T. *J. Chem. Phys.* **1973**, *59*, 3356.

(16) (a) Wolff, S. K.; Ziegler, T. *J. Chem. Phys.* **1998**, *109*, 895. (b) Wolff, S. K.; Ziegler, T.; van Lenthe, E.; Baerends, E. J. *J. Chem. Phys.* **1999**, *110*, 7689.

(17) van Lenthe, E.; Baerends, E. J.; Snijders, J. G. *J. Chem. Phys.* **1993**, *99*, 4597.

(18) (a) Baerends, E. J.; Ros, P. *Chem. Phys.* **1973**, *2*, 41. (b) te Velde, G.; Baerends, E. J. *J. Comput. Phys.* **1992**, *99*, 84. (c) Fonseca Guerra, C.; Visser, O.; Snijders, J. G.; te Velde, G.; Baerends, E. J. In *Methods and Techniques in Computational Chemistry (METECC-95)*; Clementi, E., Corongiu, G., Eds.; Cagligari, 1995; pp 305−395.

(19) (a) Snijders, J. G.; Baerends, E. J. *Mol. Phys.* **1978**, *36*, 1789. (b) Snijders, J. G.; Baerends, E. J.; Ros, P. *Mol. Phys.* **1979**, *38*, 1909. (c) Ziegler, T.; Tschinke, V.; Baerends, E. J.; Snijders, J. G.; Ravenek, W. *J. Phys. Chem.* **1989**, *93*, 3050. (d) Ziegler, T.; Snijders, J. G.; Baerends, E. J. *J. Chem. Phys.* **1981**, *74*, 1271.

(20) Schreckenbach, G.; Li, J.; Ziegler, T. *Int. J. Quantum. Chem.* **1995**, *56*, 477.

(21) Vosko, S. H.; Wilk, L.; Nusair, M. *Can. J. Phys.* **1980**, *58*, 1200.

(22) Becke, A. *Phys. Rev. A* **1988**, *38*, 3098.

(23) Perdew, J. *Phys. Rev. B* **1986**, *33*, 8822.

(24) (a) Mann, B. E. In *Annual Reports on NMR Spectroscopy*; Webb, G. A., Ed.; Academic: New York, 1994; Vol. 23, p 170. (b) Banck, J.; Schwenk, A. *Z. Phys. B* **1975**, *20*, 75. (c) Gheller, S. F.; Hambley, T. W.; Rodgers, J. R.; Brownlee, R. T. C.; O'Connor, M. J.; Snow, M. R.; Wedd, A. G. *Inorg. Chem.* **1984**, *23*, 2519. (d) Keiter, R. L.; Vander Velde, D. G. *J. Organomet. Chem.* **1983**, *258*, C34.

(25) (a) Wrackmeyer, B.; Horchler, K. In *Annual Reports on NMR Spectroscopy*; Webb, G. A., Ed.; Academic: New York, 1994; Vol. 22, p 255. (b) Kennedy, J. D.; McFarlane, W.; Pyne, G. S. *J. Chem. Soc., Dalton Trans.* **1977**, 2332. (c) Cooper, M. J.; Holliday, A. K.; Makin, P. H.; Puddephatt, R. J. *J. Organomet. Chem.* **1974**, *65*, 377. (d) Kennedy, J. D.; McFarlane, W.; Wrackmeyer, B. *Inorg. Chem.* **1976**, *15*, 1299. (e) Mitchell, T. N.; Gmehling, J.; Huber, F. *J. Chem. Soc., Dalton Trans.* **1978**, 960. (f) Hawk, R. M.; Sharp, R. R. *J. Chem. Phys.* **1974**, *60*, 1009.

(26) (a) Inorganic Crystal Structure Data Bank [ICSD, cf.: Bergerhoff, G.; Hundt, R.; Severs, P.; Brown, I. D. *J. Chem. Inf. Comput. Sci.* **1983**, *23*, 66]. Update 1995. (b) Strand, T. G. *Acta Chem. Scand.* **1994**, *48*, 960. (c) Kimura, M.; Schomaker, V.; Smith, D. W. Weinstock, B. *J. Chem. Phys.* **1968**, *48*, 4001. (d) Jost, A.; Rees, B. *Acta Crystallogr.* **1975**, *B31*, 2649.

(27) Ballhausen, C. J. In *Introduction to Ligand Field Theory*; McGraw-Hill: New York, 1962; p 149.

(28) McGlynn, S. P.; Vanquickenborn, L. G.; Kinoshita, M.; Carroll, D. G. In *Introduction to Applied Quantum Chemistry*; Holt, Reinhardt and Winston: New York, 1972.

(29) Oyamada, T.; Iijima, T.; Kimura, H. *Bull. Chem. Soc. Jpn.* **1971**, *44*, 2638.